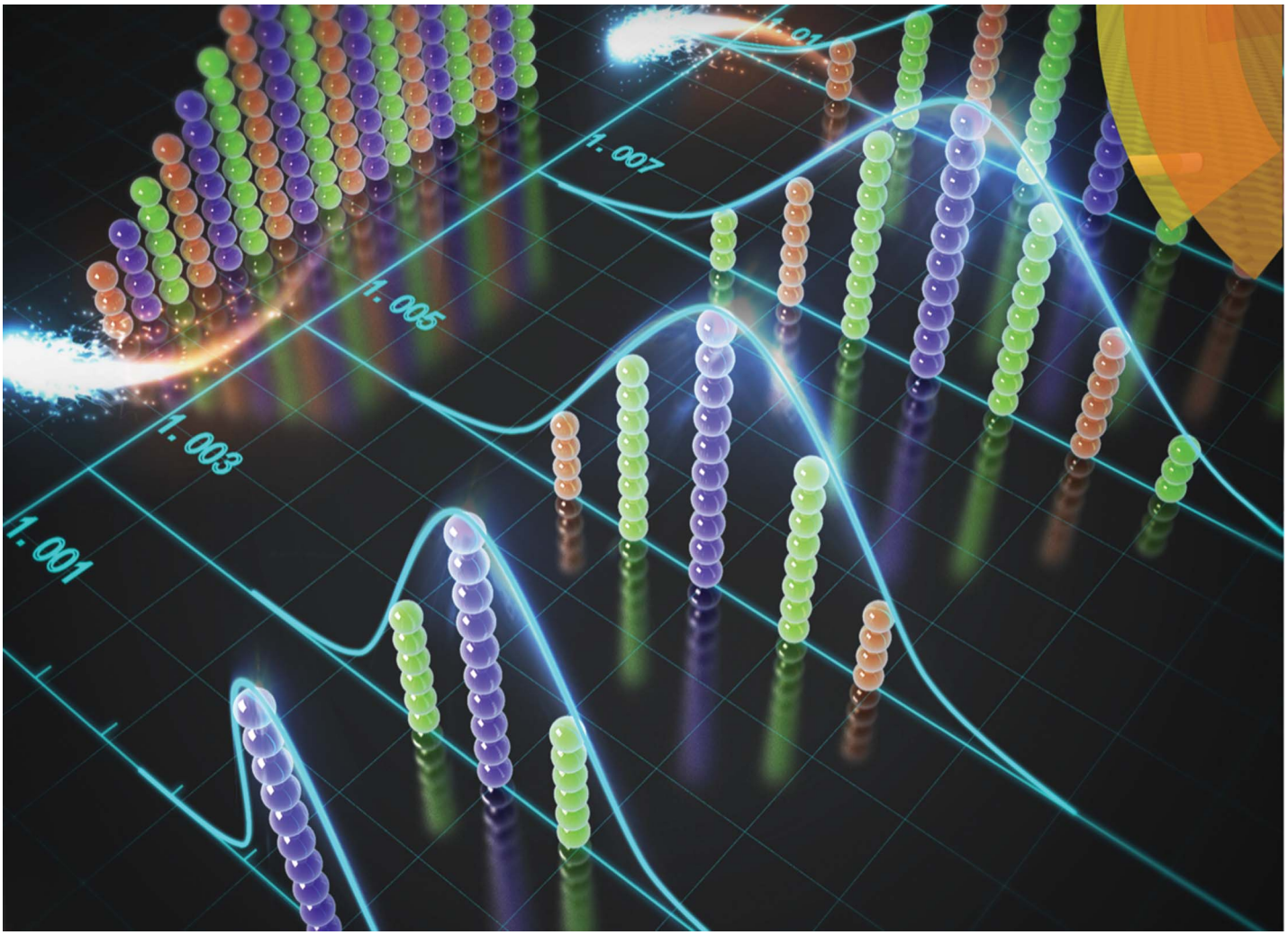

Showcasing research from Professor Xue-Hui Dong's laboratory, School of Molecular Science and Engineering, South China University of Technology, Guangzhou, China.

Precise modulation of molecular weight distribution for structural engineering

Molecular weight is one of the most fundamental parameters defining a polymer. The structure and properties of polymeric materials depend not only on average molecular weight, but also on the distribution of molecular weight. Quantitative and comprehensive understanding on the importance of molecular weight distribution is, however, still unclear. We demonstrated a robust and effective approach to artificially engineer molecular weight distribution through precise blending of discrete macromolecules. This work could bridge the gap between discrete and dispersed macromolecules, providing fundamental perspectives on the critical role of molecular weight distribution.

As featured in:

See Xue-Hui Dong *et al.*, *Chem. Sci.*, 2019, **10**, 10698.

ROYAL SOCIETY OF CHEMISTRY | Celebrating IYPT 2019

rsc.li/chemical-science

Registered charity number: 207890

Chemical Science

EDGE ARTICLE

View Article Online
View Journal | View Issue

Cite this: *Chem. Sci.*, 2019, **10**, 10698

All publication charges for this article have been paid for by the Royal Society of Chemistry

Precise modulation of molecular weight distribution for structural engineering†

Rui Tan,[a] Dongdong Zhou,[a] Baolei Liu,[c] Yanxiao Sun,[a] Xinxin Liu,[a] Zhuang Ma,[a] Deyu Kong,[a] Jinlin He,[c] Zhengbiao Zhang[c] and Xue-Hui Dong *[ab]

Received 20th September 2019
Accepted 28th October 2019

DOI: 10.1039/c9sc04736k

rsc.li/chemical-science

As one of the most critical molecular parameters, molecular weight distribution has a profound impact on the structure and properties of polymers. Quantitative and comprehensive understanding, however, has yet to be established, mainly due to the challenge in the precise control and regulation of molecular weight distribution. In this work, we demonstrated a robust and effective approach to artificially engineer the molecular weight distribution through precise recombination of discrete macromolecules. The width, symmetry, and other characteristics of the distribution can be independently manipulated to achieve absolute control, serving as a model platform for highlighting the importance of chain length heterogeneity in structural engineering. Different from their discrete counterparts, each individual component in dispersed samples experiences a varied degree of supercooling at a specific crystallization temperature. Non-uniform crystal nucleation and growth kinetics lead to distinct molecular arrangements. This work could bridge the gap between discrete and dispersed macromolecules, providing fundamental perspectives on the critical role of molecular weight distribution.

Introduction

Molecular weight is one of the most fundamental parameters that define a macromolecule. Unlike most biomacromolecules of uniform size, synthetic macromolecules generally have an inherent heterogeneity in their chain length. Many behaviors of polymeric materials, such as viscosity, processability, crystallization, and self-assembly, depend not only on the average molecular weight, but also on the distribution of molecular weight.[1] Minor changes in the distribution could significantly alter the content of each component, which may result in substantial differences in the physical properties.[2] Although a few pioneering theoretical explorations[3–7] and experimental studies[8–14] have been conducted, the importance of molecular weight distribution in determining the structure and properties of macromolecules is, however, still unclear. There are mainly two obstacles: (i) precise control and quantitative modulation of molecular weight distribution is challenging;[13,15,16] and (ii) molecular weight distribution is a complex parameter consisting of multiple variables such as distribution width, symmetry, shape, *etc.*[17] The collective effect is very difficult to decouple to elucidate the independent contribution of each factor.[12,18]

A polymer is essentially a mixture of macromolecules having the same repeat unit and consecutive degrees of polymerization. Average molecular weight (*e.g.* number average, M_n, or weight average, M_w) and dispersity ($Đ$, defined as M_w/M_n), measured typically by size exclusive chromatography (SEC), however, provide only indirect and oversimplified characteristics of the composition (*i.e.* arithmetic mean and relative breadth of the distribution).[18] Samples with the same M_n and $Đ$ do not necessarily have the same constitution.[12] In principle, higher moments (such as *skewness* and *kurtosis*) containing information about symmetry, shape, *etc.* of a given distribution are also required.[17,19] These critical quantities, however, are usually not included in $Đ$. Therefore, $Đ$ is not a comprehensive description of molecular weight distribution.[18] The use of $Đ$ as a sole variable to represent the molecular weight distribution could thus be limited.

Technically, two approaches are usually adopted to modulate molecular weight distribution.[20] One is to control the polymerization process. The development of living/controlled polymerization makes complicated molecular design and "narrow" molecular weight distribution possible.[21–23] Recently, Fors[13,24] and Cölfen[15] further demonstrated initial attempts to control the shape of the molecular weight distribution by manipulating the initiation process, such as temporal control of the initiator addition, or spatial

[a]South China Advanced Institute of Soft Matter Science and Technology, School of Molecular Science and Engineering, South China University of Technology, Guangzhou 510640, China. E-mail: xdong@scut.edu.cn

[b]State Key Laboratory of Luminescent Materials and Devices, South China University of Technology, Guangzhou 510640, China

[c]College of Chemistry, Chemical Engineering and Materials Science, Soochow University, Suzhou, 215123, China

† Electronic supplementary information (ESI) available: Synthesis and characterization of discrete and dispersed samples. See DOI: 10.1039/c9sc04736k

control of the initiator gradient. Though the molecular weight distribution can be regulated to some extent,[25–27] precise control is not possible due to the essential statistical nature of chain growth. The batch-to-batch variation would severely impede further systematic studies. The second approach is to blend samples with different average molecular weights.[28–30] Although this method is relatively simple and straightforward, the resultant blends suffer from complex compositions such as multimodal distributions, due to the intrinsic chain length heterogeneity of the blending stocks.

Precise control and modulation of molecular weight distribution is the prerequisite for quantitative and comprehensive exploration. Discrete polymers ($Đ = 1$) having a definite composition, sequence, and topology exhibit unique phase behaviors compared to their dispersed analogues,[31,32] revealing high sensitivity of microstructures to the chain length heterogeneity.[33–39] In this study, we will demonstrate a method for precisely tailoring the molecular weight distribution. By rationally blending discrete *oligo*-L-lactic acid (*o*LLA) according to certain distribution functions (such as the *Schulz–Zimm* distribution, *Gaussian* distribution, *skew-normal* distribution, *etc.*), we could artificially generate and regulate molecular weight distributions on demand (Scheme 1a). The content of each component is accurately defined, and the width, symmetry, shape, and other characteristics of molecular weight distribution could be independently engineered to achieve absolute control, bridging the gap between discrete and dispersed macromolecules. Crystallization behaviors of *o*LLAs with varied distributions are systematically studied and quantitatively compared (Schemes 1b and c), serving as a model example to reveal the detailed contribution of molecular weight distribution. This research work not only deepens the understanding of fundamental crystallization theory, but also provides a potential tunable molecular parameter for rational design of functional polymers with advanced properties.

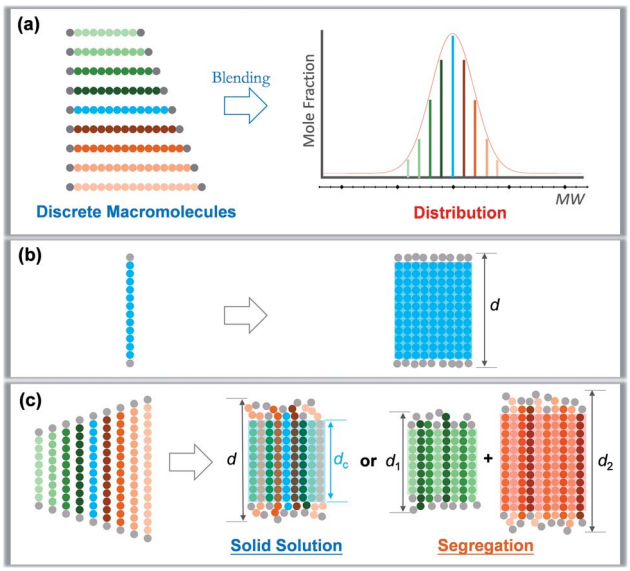

Scheme 1 Modulation of molecular weight distribution *via* precisely blending discrete macromolecules (a) and proposed molecular packing of discrete (b) and dispersed (c) *o*LLAs upon crystallization.

Results and discussion

Synthesis of discrete *o*LLAs

Discrete *o*LLAs were synthesized following an iterative growth route (Scheme S1, see the ESI† for details).[40,41] The oligomers have *tert*-butyldimethylsilyl (TBDMS) and benzyl (Bn) groups as two protecting end groups, respectively (Fig. 1a). Discrete *o*LLAs with the number of repeat units ranging from 12 to 32 were prepared typically at the gram scale (labeled as $oLLA_x$, where x refers to the number of repeat units). Their chemical structure was characterized by proton nuclear magnetic resonance (^{1}H NMR, Fig. S1†). For each sample, matrix-assisted laser desorption/ionization time-of-flight mass spectrometry (MALDI-ToF MS) displays a single peak with molecular weight in good accordance with the calculated value, confirming the identity and discrete feature (Fig. 1b and S3†). Size exclusive chromatography (SEC) elution profiles show a certain instrumental spread though the samples have uniform size, which can be attributed to diffusion in the column (Fig. S2a†). Though no further attempt has been made, it should also be possible to prepare *o*LLA with higher molecular weight by taking advantage of the exponential growth approach. Detailed molecular information of the discrete *o*LLA library is summarized in Table S1.†

Crystallization behaviors of discrete *o*LLAs

All the *o*LLA samples listed in Table S1† are crystalline solids at room temperature. It is well known that poly(L-lactic acid) has

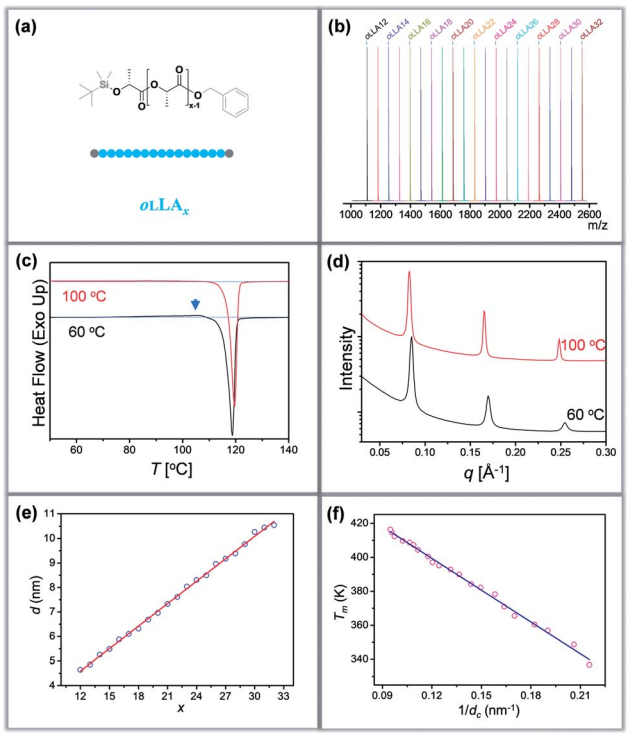

Fig. 1 (a and b) Chemical structure (a) and combined MALDI-ToF mass spectra (b) of discrete oLLAs. (c and d) Representative DSC thermograms (c) and SAXS profiles (d) of discrete $oLLA_{22}$ crystallized at 60 °C (black) and 100 °C (red). (e and f) Correlation between lamellar thickness and number of repeat units (e), and between melting temperature and crystal thickness (f).

multiple crystal polymorphs, in which the α form with two 10_3 helical chains packed into an orthorhombic unit cell is the most common one.[42] An α' form has recently been recognized as a "disordered crystal" having the same 10_3 helical conformation but a loose packing structure, which is likely to be produced at low crystallization temperature (T_c).[43,44] Similar behaviors were also recorded in the oligomers. As will be clarified later, discrete *o*LLAs assume α' form and metastable α form crystals at relatively high supercooling. To avoid potential polymorphism and/or kinetic trapping, an isothermal crystallization process, with T_c being about 20 °C below the melting temperature (T_m) of each discrete *o*LLA, was adopted (see the ESI† for details).

All the *o*LLAs that crystallized under the above-mentioned conditions are in the α crystal form, as confirmed by differential scanning calorimetry (DSC) and wide-angle X-ray diffraction (WAXD). In general, a single and sharp endothermic melting can be observed in the DSC thermograms (Fig. 1c, red), corresponding to the melting transition of *o*LLA crystals possessing highly ordered packing. Due to the low molecular weight nature, T_m is very sensitive to the chain length variation, covering a broad temperature range (Fig. S4 and Table S1†). Three characteristic diffraction peaks can be observed at $2\theta =$ 14.8, 16.7, and 19.1° (Fig. S6b,† red), corresponding to (010), (110)/(200), and (203) planes of the orthorhombic unit cells of the α form crystal, with two 10_3 helical chains parallel to the *c* axis (also parallel to the normal of the lamellae).[42]

Small angle X-ray scattering (SAXS) patterns exhibit sharp scattering peaks with a ratio of 1 : 2 : 3 : 4…, which are typical characteristics of a highly uniform lamellar structure (Fig. 1d and S5†).[35] The lamellar thickness (d, determined by the primary peak of the SAXS pattern) increases as the number of repeat units increases, with a near-perfect linear correlation (Fig. 1e and Table S1†), indicating that all these crystals adopt an extended chain conformation (Scheme 1b).[36] Extrapolating the linear fit to $x = 0$ gives the thickness of the amorphous layer ($d_a = 0.91$ nm, mainly the protecting group, assuming 100% crystallinity), and the thickness of the crystalline layer (d_c) can thus be calculated accordingly ($d_c = d - d_a$). The slope of the linear fit, on the other hand, indicates an increase of 0.307 ± 0.003 nm per monomeric residue, which is in good agreement with the crystal unit cell parameters.[36]

For polymer lamellar crystals, the relationship between T_m and d_c can be described by the Thomson–Gibbs equation (eqn (1))

$$T_m = T_{m,0}\left(1 - \frac{2\gamma_e}{d_c \Delta H_f}\right) \quad (1)$$

where $T_{m,0}$ is the equilibrium melting temperature of the crystal with an infinite size, γ_e is the surface free energy of the crystal, and ΔH_f is the equilibrium heat of fusion. The linear correlation between T_m and $1/d_c$ is shown in Fig. 1f. The intercept gives the equilibrium melting temperature $T_{m,0} = 474$ K (*i.e.* 201 °C), close to that reported in the literature (215 °C).[45] The difference might originate from the semi-crystalline nature of polymers that cannot reach 100% crystallinity.

It should be noted that these extended chain crystals are not always under thermodynamic equilibrium. Typical α' form crystals were produced when crystallized at a relatively low temperature, as revealed by a small exotherm in the DSC thermogram prior to the dominant melting peak (Fig. 1c and S5a,† indicated by an arrow, corresponding to an α'-to-α form transition). WAXD patterns further corroborate the formation of the α' form crystal by a slight shift of the (110)/(200) and (203) diffractions toward lower angles, as well as the disappearance of (103) and other diffractions (Fig. S6b†). Other metastable states (*i.e.*, ill-defined α form crystals) were also captured at large x and/or high supercooling, as indicated by the additional melting transitions in the DSC thermograms (Fig. S4†), attributed probably to kinetic trapping.[42] Nevertheless, neither is the lamellar thickness nor the corresponding equilibrium T_m sensitive to the crystallization conditions (Fig. 1d and S5a†), due to extended chain conformation and very similar unit cells between α and α' form crystals. The clear and quantitative correlations make this library of molecules a unique platform to reveal the profound importance of dispersity in polymer crystallization.

Modulation of molecular weight distribution

Blending discrete species according to specific recipes provides an effective and straightforward strategy to precisely manipulate the width and shape of the molecular weight distribution. As the simplest case, a symmetric distribution can be generated based on the *Gaussian* distribution (Scheme S2a†). For a given $Đ$ and M_n, the molar content of each component ($n(x)$) can be determined using eqn (2) and (3)

$$n(x) = \frac{1}{\sqrt{2\pi\sigma^2}} e^{-\frac{(M_x - M_n)^2}{2\sigma^2}} \quad (2)$$

$$\left(\frac{\sigma}{M_n}\right)^2 = Đ - 1 \quad (3)$$

where σ is the standard deviation and M_x is the molecular weight of *o*LLA$_x$. A series of samples with the same M_n ($x = 19$, 22, or 24) and varying $Đ$ ($Đ = 1.001$, 1.003, 1.005, 1.007, 1.01, 1.02, 1.04, 1.06, and 1.10) were prepared accordingly. UV absorption was used for calibration to achieve high precision (see the ESI†). Detailed compositions for each sample series are listed in Table S2.†

The resultant blends are characterized by SEC and MALDI-ToF MS. Here we take the *o*LLA$_{22}$ series as an example. Minor adjustments of $Đ$ can be clearly distinguished by SEC (Fig. 2a and S7†). M_n and $Đ$ were experimentally calculated based on SEC profiles using the discrete *o*LLA library for calibration, exhibiting a constant average and an increasing dispersity (Table 1). Samples with low $Đ$ generally have a near-perfect bell shape, while those with larger $Đ$ show a tail on the low molecular weight side (Fig. S8a†). This deviation originates from the nonlinear correlation between the retention time and the molecular size (Fig. S2b†). It should be noted that the SEC curves in Fig. 2a are not a simple resemblance of the *Gaussian* distribution (Scheme S2a†), since they have different coordinate axes (molecular weight *vs.* retention time). In principle, a mathematical representation of the *Gaussian* distribution in

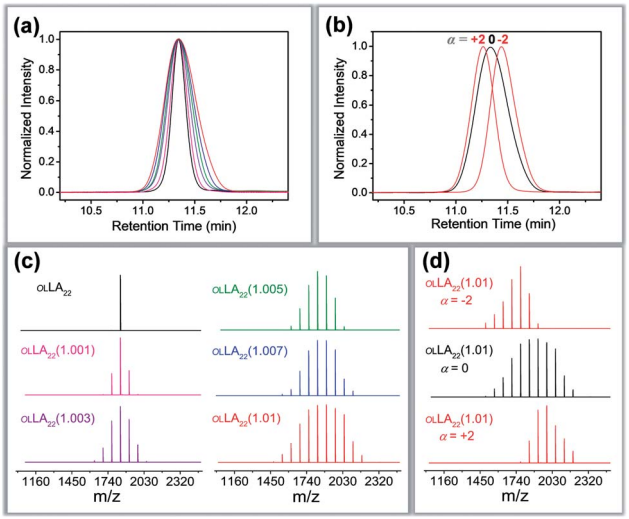

Fig. 2 SEC traces (a and b) and the corresponding MALDI-ToF mass spectra (c and d) of symmetrically (a and c) and asymmetrically (b and d) dispersed oLLA$_{22}$ series samples (Tables 1 and 2). For clarity, only $Đ$ = 1.00–1.01 and $\alpha = \pm 2$ are shown. See Fig. S8† for more data.

the semilogarithmic coordinates (corresponding to retention time) would not be symmetric. Diffusion, however, would smooth the SEC traces, making them appear symmetric in the case of limited $Đ$. MALDI-ToF MS, on the other hand, provides improved resolution of the composition. Typical mass spectra are shown in Fig. 2c and S8c†. Each of the fractions in the formulation can be recognized, and their relative ratio can be clearly identified. Due to the difference of ionization efficiency, the intensity corresponding to each fraction might deviate from the actual composition. Nevertheless, a *Gaussian* distribution is evident in general, and resembles the mathematical calculation more appropriately. The same characteristics were also observed in the *o*LLA$_{19}$ and *o*LLA$_{24}$ series (Fig. S9 and S10†). Detailed characterization is summarized in Table S4.†

$$n(x) = \frac{1}{\sqrt{2\pi\sigma^2}} e^{-\frac{(M_x - M_n)^2}{2\sigma^2}} \int_{-\infty}^{\frac{\alpha(M_x - M_n)}{\sigma}} \frac{1}{\sqrt{2\pi}} \exp\left(-\frac{t^2}{2}\right) dt \quad (4)$$

To generate an asymmetric molecular weight distribution, we adopted the *skew-normal* distribution (eqn (4)) as a proof of concept, by introducing an additional asymmetric parameter, α (Scheme S2b†).

The *skew-normal* distribution will be reduced to a *Gaussian* distribution (eqn (2)) when $\alpha = 0$, while it will skew to higher or lower molecular weight when α is a positive or negative integer, respectively (Scheme S2b†). We prepared three sets of blending samples with fixed M_n (x = 19, 22, or 24) and $Đ$ ($Đ$ = 1.01), while tuning the value of α. Detailed compositions are listed in Table S3.†

Fig. 2b and d show the SEC traces and MALDI-ToF mass spectra of the resultant asymmetric *o*LLA$_{22}$ series. Compared with a *Gaussian* distribution, clear deviations from a symmetric curve can be observed when α is not 0 (Fig. 2b). The SEC traces incline to the lower retention time (higher M_w) when α is positive, while they incline to the larger retention time (lower M_w) when α is negative. The initial change in the symmetry is apparent (*e.g.*, from $\alpha = 0$ to $\alpha = \pm 1$), while a further increase in α generates a mild variation (Fig. S8†). It should be noted that the average molecular weight and dispersity inevitably drift when α is introduced, despite the fact that M_n and σ were set as constant in eqn (4). Using the discrete *o*LLA library for calibration, effective M_n and $Đ$ were measured and the results are listed in Table 2, which fit well to calculations based on the constitution (see the ESI†). MALDI-ToF MS provides detailed information of the composition (Fig. 2d). Each individual peak can be assigned to the ingredient in the blending formulation. The relative abundance is proportional to the peak intensity qualitatively, resembling the features of the *skew-normal* distribution in general. The same characteristics were also recorded in the *o*LLA$_{19}$ and *o*LLA$_{24}$ series (Fig. S9 and S10 and Table S5†). The precise composition confirms the blending

Table 1 Molecular characterization of symmetrically dispersed *o*LLA samples

				T_c^f = 60 °C			T_c^f = 100 °C					
Sample[a]	M_n[b]	$Đ$		d[g]	T_m[h]	ΔH_m[i]	d_1[g]	$T_{m,1}$[h]	$\Delta H_{m,1}$[i]	d_2[g]	$T_{m,2}$[h]	$\Delta H_{m,2}$[i]
*o*LLA$_{22}$[e]	1807.8[e]	<1.0001[e]		7.57	119.1	64.8	7.57	119.7	73.5	—	—	—
*o*LLA$_{22}$(1.001)	1800	1.003[c]	1.001[d]	7.39	118.4	57.5	7.57	118.7	66.0	—	—	—
*o*LLA$_{22}$(1.003)	1810	1.005	1.002	7.48	117.2	54.1	7.57	117.4	57.1	—	—	—
*o*LLA$_{22}$(1.005)	1810	1.006	1.002	7.48	116.5	50.0	7.57	116.7	58.8	—	—	—
*o*LLA$_{22}$(1.007)	1820	1.007	1.004	7.48	116.0	40.9	7.57	116.0	58.7	—	—	—
*o*LLA$_{22}$(1.01)	1800	1.009	1.006	7.57	115.9	45.6	7.66	115.9	61.9	—	—	—
*o*LLA$_{22}$(1.02)	1800	1.012	1.009	7.48	115.3	41.7	7.66	115.1	54.2	—	—	—
*o*LLA$_{22}$(1.04)	1800	1.029	1.015	7.65	115.2	42.7	7.85	115.2	48.8	6.16	83.6	3.0
*o*LLA$_{22}$(1.06)	1790	1.038	1.024	7.73	115.0	37.1	8.06	119.6	43.4	6.10	82.4	5.3
*o*LLA$_{22}$(1.10)	1780	1.050	1.027	7.86	114.8	39.2	8.27	121.7	38.8	5.87	82.0	7.3

[a] Sample label *o*LLA$_x$($Đ$), where x refers to the number of repeat units and $Đ$ is the dispersity. [b] Number average molecular weight (Da) measured by SEC using the discrete *o*LLA library for calibration. [c] Dispersity measured by SEC using the discrete *o*LLA library for calibration. [d] Dispersity measured by MADLI-ToF. [e] Discrete *o*LLA$_{22}$, adopted from Table S1. [f] Crystallization temperature (T_c). [g] Lamellar thickness, nm, calculated based on $d = 2\pi/q^*$. [h] Melting temperature (°C), determined by DSC. [i] Heat of fusion (J g^{-1}), determined by DSC.

Table 2 Molecular characterization of asymmetrically dispersed *o*LLA samples

Sample[a]	M_n[b]	$Đ$		d[e]	T_m[f]	ΔH_m[g]
$o\text{LLA}_{22}(-3)$	1650	1.007[c]	1.003[d]	7.06	109.4	51.6
$o\text{LLA}_{22}(-2)$	1660	1.008	1.003	7.22	110.2	54.1
$o\text{LLA}_{22}(-1)$	1680	1.009	1.005	7.30	112.1	55.4
$o\text{LLA}_{22}(0)$	1800	1.009	1.006	7.57	116.0	60.8
$o\text{LLA}_{22}(+1)$	1880	1.008	1.003	7.95	118.9	61.7
$o\text{LLA}_{22}(+2)$	1900	1.008	1.003	8.06	119.8	64.3
$o\text{LLA}_{22}(+3)$	1910	1.006	1.002	8.16	121.1	64.6

[a] Sample label $o\text{LLA}_x(\alpha)$, where x refers to the number of repeat units and α is the asymmetric parameter. [b] Number average molecular weight (Da) measured by SEC using the discrete *o*LLA library for calibration. [c] Dispersity measured by SEC using the discrete *o*LLA library for calibration. [d] Dispersity measured by MADLI-ToF. [e] Lamellar thickness, nm. [f] Melting temperature (°C), determined by DSC. [g] Heat of fusion (J g^{-1}), determined by DSC. T_c = 80 °C.

strategy as a robust and efficient approach in tailoring the width and shape of the molecular weight distribution.

Effects of distribution width on crystallization

A synthetic polymer contains a collection of non-uniform macromolecules with size-dependent behaviors. The structure and properties are collective and synergistic outputs of each individual component. As for crystallization, organizing polymer chains into an ordered arrangement critically depends on supercooling (*i.e.*, $\Delta T = T_m - T_c$).[46] Different from a discrete polymer with an explicit melting temperature, a dispersed polymer consists of multiple fractions, for which T_m usually covers a broad range of temperatures. As a result, at a specific crystallization temperature, each individual species may experience a varied degree of supercooling, leading to non-uniform nucleation and growth kinetics. As $Đ$ increases, the disparity on supercooling may result in three possible scenarios during crystallization (Scheme 1c): (1) solid solution, that is polymer chains with different lengths co-crystallize homogeneously; (2) eutectic system, that is one (or some) component(s) crystallizes partially from miscible melts before reaching the eutectic point, beyond which the remaining melts co-crystallize; and (3) segregation, in which polymer chains separate into different domains based on chain length.[47,48] Detailed molecular packing, however, has yet to be quantitatively explored due to the challenge in dispersity modulation.

It can be envisioned that crystallization temperature plays vital role in the molecular arrangement. By defining the equilibrium melting temperature of the longest and shortest components of a dispersed sample as T_m^H and T_m^L respectively, three temperature regions can be recognized: full crystallization (all the fractions participate in the crystallization) is expected when $T_c < T_m^L$ (region I); partial crystallization takes place for $T_m^L < T_c < T_m^H$ (region II); and no crystallization occurs when $T_c > T_m^H$ (region III).

Take the symmetrically dispersed $o\text{LLA}_{22}$ series (Table 1) as an example. The T_m^H and T_m^L of each sample are listed in Table S6.† To systematically explore the crystallization behaviors, the $o\text{LLA}_{22}$ series with varying $Đ$ were isothermally crystallized at a set of temperatures (T_c = 60, 80, 100, and 110 °C) for sufficient time before cooling to room temperature. The as-prepared solids were then characterized by DSC, SAXS, and WAXD.

Different crystallization characteristics were recorded in region I and region II. In the case of T_c = 60 °C, all the samples are crystallized in region I. A set of sharp and equally spaced scattering peaks were observed for each sample, similar to the SAXS profile of discrete $o\text{LLA}_{22}$ (Fig. 3a). The position of the peaks remains nearly constant (very slightly to the left), indicating that the lamellar thickness is not significantly affected by the chain length heterogeneity. The uniformity of the lamellae, on the other hand, diminishes as $Đ$ increases, as revealed by the broadening of the primary peak (Fig. 3a). Similar behaviors were recorded at T_c = 80 °C.

In the case of T_c = 100 °C, $o\text{LLA}_{22}$ series samples with $Đ$ < 1.02 are still in region I, while those with $Đ \geq 1.02$ enter region II. The former show essentially the same SAXS patterns as those of samples crystallized at 60 °C (Fig. 3b). For samples with $Đ \geq$ 1.02, an obvious shift of the peaks to the left was observed (Fig. 3b, solid red triangles), accompanied by the appearance of an additional set of equally spaced scattering peaks (Fig. 3b, open red triangles, not detected in the case of $Đ$ = 1.02 due to the trace amount of low molecular weight fractions). Similar behaviors were recorded at T_c = 110 °C. The relationship between lamellar thickness (d) and $Đ$ at different T_c is plotted in Fig. 3c (see Fig. S11† for more data).

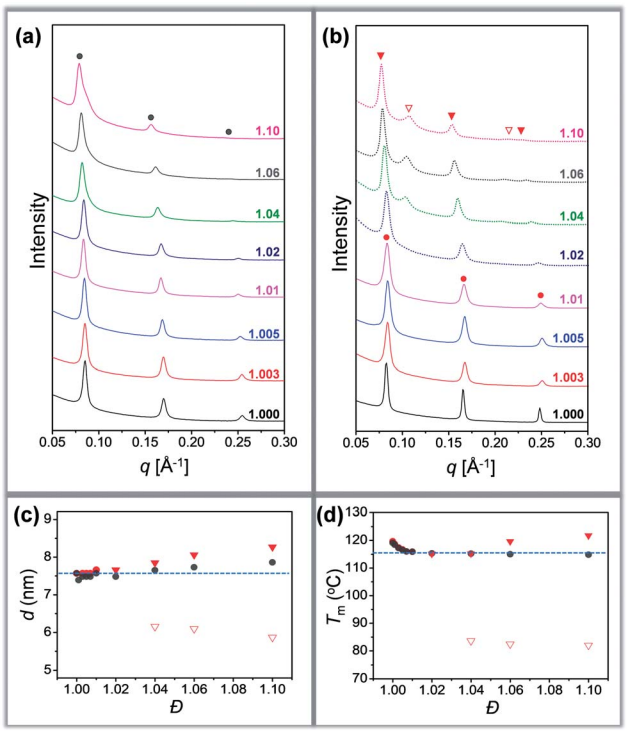

Fig. 3 (a and b) SAXS patterns of $o\text{LLA}_{22}$ series samples with varying $Đ$ crystallized at 60 °C (a) and 100 °C (b): solid line (region I); dashed line (region II). (c and d) Relationship between lamellar thickness and $Đ$ (c), and between melting temperature (T_m) and $Đ$ (d): solid circles (region I); triangles (region II). Only T_c = 60 °C (grey) and 100 °C (red) are shown for clarity. See Fig. S11† for more data.

We propose that *o*LLA chains align in an extended conformation perpendicular to the lamellar surface, unaffected by chain length heterogeneity or crystallization conditions. The detailed molecular packing, however, depends critically on both T_c and $Đ$. The uniform lamellae thickness in region I indicates that *o*LLAs co-crystallize homogeneously to form solid solutions (Scheme 1c). The existence of multiple populations of lamellae in region II, on the other hand, is due to the segregation of the *o*LLA chains with varying chain length: long chains crystallize, while short chains remain in the melt and crystallize upon further cooling to room temperature (Scheme 1c). No eutectic behavior was observed.

The resultant lamellae consist of alternating crystalline and amorphous layers. The overall lamellar thickness (d) is a sum of both contributions ($d = d_a + d_c$), which can be calculated based on eqn (5)

$$d = \frac{M_n}{N_A(\rho_c f_c + \rho_a f_a) \times s} \quad (5)$$

where s is the cross-sectional area of each *o*LLA stem, N_A is the Avogadro constant, ρ and f are the density and volume fraction, and subscripts c and a refer to the crystalline and amorphous layers, respectively. It is evident that the average molecular weight (M_n), rather than dispersity ($Đ$), dictates the lamellar thickness (d). In region I, all the fractions were involved in crystallization, and M_n is essentially constant despite varying $Đ$. The slight increase of d is attributed to the reduction of crystallinity as $Đ$ increases (Table 1). A minor difference between ρ_a and ρ_c (1.25 *vs.* 1.29 g cm^{-3})[49] results in a slight thickening of d. In region II, the effective M_n of the crystallizable fractions significantly increases, as low molecular weight fractions are excluded from the crystal, which results in a sudden increase of d (solid triangle, Fig. 3c), as well as an additional population of lamellae that crystallize upon further cooling to room temperature. With increasing dispersity, the thickness of the newly formed crystals continuously decreases (open triangle, Fig. 3c), due to the increasing fraction of short chain components.

Detailed molecular packing is further revealed by DSC and WAXD. According to the proposed molecular arrangement, a single endothermic peak is expected in the DSC thermogram in region I, while two separate peaks are expected in region II, corresponding to each individual lamella population. This feature is generally followed (Fig. S12†). There, however, also exist some additional peaks, especially when $Đ$ is relatively large. For example, the DSC curve of the discrete sample crystallized at 60 °C shows a sharp melting peak in the DSC thermogram. As $Đ$ increases, an exothermic peak appears before the melting peak. The exotherm becomes broad as $Đ$ further increases, followed by the melting process with multiple overlapping peaks (Fig. S12†). Though they look complicated, the characteristics have been well-recognized in the crystallization of PLLA, due to co-existence of multiple metastable crystals.[44] The exotherm is attributed to the α'-to-α form transition (see WAXD data in Fig. S13†), while the latter corresponds to a series of melting–recrystallization processes. Metastable crystals (*e.g.*, with defects included inside, varying crystal thickness, *etc.*) generated under non-uniform supercooling are continuously annealed and rearranged during the heating process, resulting in multiple endothermic peaks.[44] The rearrangement, however, does not change the overall lamellar thickness (d), as confirmed by the SAXS patterns of samples annealed at elevated temperatures (Fig. S14†). By assuming the highest melting peaks as the equilibrium melting point of dispersed samples, the relationship between T_m and $Đ$ was established (Fig. 3d). A depression of T_m, accompanied by a reduction of crystallinity (Table 1), was recorded as $Đ$ increases, indicating the shrinking of the crystalline layer (d_c). In the case of region II, an additional melting peak appears as expected, corresponding to the melting transition of the low molecular weight fractions (Fig. S12,† open triangle). All the data are summarized in Table 1. The DSC data (Fig. 3d) generally follow a similar trend to the SAXS results (Fig. 3c). Parallel studies on the *o*LLA$_{19}$ and *o*LLA$_{24}$ series samples show essentially the same behaviors (Table S4 and Fig. S15–S18†), further supporting our proposed molecular arrangement.

Effects of distribution symmetry on crystallization

The symmetry is another characteristic of molecular weight distribution dictating the composition. Our understanding in this area is, however, still in the primitive stage.[12,13] The asymmetrically dispersed samples prepared in this work could provide a model system to elucidate the contribution of distribution symmetry.

Take the *o*LLA$_{22}$ series ($Đ = 1.01$, see Table 2) with varying skewness as examples. All these samples were isothermally crystallized at 80 °C (region I). A homogeneous solid solution forms under these conditions, as revealed by a set of equally spaced scattering peaks in the scattering profile (Fig. S19a†), as well as a single melting peak in the DSC thermogram (Fig.-S19b†). Compared with the symmetrically dispersed counterpart, *i.e.* *o*LLA$_{22}$(1.01), both lamellar thickness (d) and melting temperature (T_m) are significantly altered by variation of α (Table 2). In general, d and T_m increase simultaneously and monotonically when $\alpha > 0$, while they decrease when $\alpha < 0$ (Fig. 4). Similar behaviors were also recorded for the *o*LLA$_{19}$ and *o*LLA$_{24}$ series samples (Table S5† and Fig. S20 and S21†).

As revealed by eqn (5), d (as well as equilibrium T_m) is dictated by the average molecular weight. The shift of effective

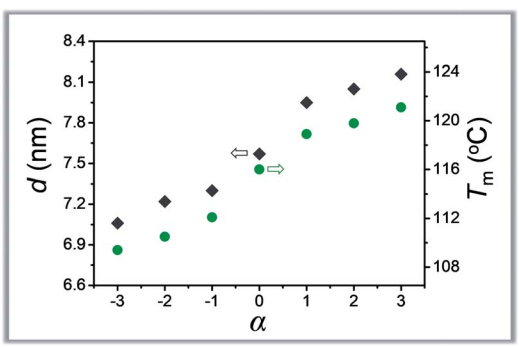

Fig. 4 Plot of lamellar thickness (grey) and melting temperature (olive) of asymmetrically dispersed *o*LLA$_{22}$ samples as a function of α.

M_n results in the change of d and T_m in the same direction. On the other hand, samples with similar M_n and $Đ$ but different symmetries [*e.g.*, $o\mathrm{LLA}_{22}(1.01, \alpha = +2)$ *vs.* $o\mathrm{LLA}_{24}(1.01)$] exhibit similar lamellar thickness (Fig. S22a†). This, however, does not necessarily imply that the shape of the distribution has no impact on crystallization. On the one hand, lamellar thickness is an average property which is not sensitive to the heterogeneity of the chain length (neither width nor symmetry, eqn (5)). On the other hand, the samples involved in this section generally have relatively low dispersity ($Đ = 1.01$), which cannot generate appreciable differences. Nevertheless, a quite different melting transition was recorded (Fig. S22b†), indicating that detailed molecular packing is influenced by the symmetry of the distribution. We envision that the contribution of the asymmetric composition is more profound in the processes that depend critically on individual performance, especially crystallization kinetics. The details will be discussed in a separate study.

Conclusions

In this work, we established an efficient approach to modulate molecular weight distribution through precise recombination of discrete macromolecules. A series of dispersed *o*LLA samples were prepared accordingly with tailored average, width, and symmetry. The profound influence of molecular weight distribution on crystallization behaviors was quantitatively studied. Depending on crystallization temperature, *o*LLAs in dispersed samples adopt distinct molecular arrangements, *i.e.*, solid solution or segregation, due to non-uniform nucleation and growth kinetics. The blending strategy is very robust, and can be extended to regulate the chain length heterogeneity of one or multiple blocks of block copolymers or polymers with complicated architectures. In principle, arbitrary distributions could be constructed at will, including those inaccessible through polymerization. It thus provides a unique model platform to elucidate the critical contribution of chain length heterogeneity to self-assembly and molecular dynamics, as well as properties of polymers.

Conflicts of interest

There are no conflicts to declare.

Acknowledgements

This work was supported by the National Natural Science Foundation of China (51773066), the Guangdong Innovative and Entrepreneurial Research Team Program (2016ZT06C322), and the Fundamental Research Funds for the Central Universities (2019XX04). We thank the staff of Beamline BL16B1 at the Shanghai Synchrotron Radiation Facility for assistance with the SAXS experiments.

Notes and references

1 D. W. van Krevelen and K. te Nijenhuis, *Properties of Polymers*, Elsevier, Amsterdam, 2009.
2 W. Zhang, X. Dong and S. Z. Cheng, *Chem*, 2019, **5**, 492.
3 L. Leibler, *Macromolecules*, 1980, **13**, 1602.
4 D. M. Cooke and A.-C. Shi, *Macromolecules*, 2006, **39**, 6661.
5 N. A. Lynd, M. A. Hillmyer and M. W. Matsen, *Macromolecules*, 2008, **41**, 4531.
6 B. L. Peters, M. K. Salerno, T. Ge, D. Perahia and G. S. Grest, *Phys. Rev. Lett.*, 2018, **121**, 057802.
7 P. K. Bommineni, N. Varela-Rosales, M. Klement and M. Engel, *Phys. Rev. Lett.*, 2019, **122**, 128005.
8 N. A. Lynd and M. A. Hillmyer, *Macromolecules*, 2005, **38**, 8803.
9 N. A. Lynd and M. A. Hillmyer, *Macromolecules*, 2007, **40**, 8050.
10 N. A. Lynd, A. J. Meuler and M. A. Hillmyer, *Prog. Polym. Sci.*, 2008, **33**, 875.
11 J. M. Widin, A. K. Schmitt, A. L. Schmitt, K. Im and M. K. Mahanthappa, *J. Am. Chem. Soc.*, 2012, **134**, 3834.
12 D. T. Gentekos, J. Jia, E. S. Tirado, K. P. Barteau, D.-M. Smilgies, R. A. Distasio and B. P. Fors, *J. Am. Chem. Soc.*, 2018, **140**, 4639.
13 D. T. Gentekos, L. N. Dupuis and B. P. Fors, *J. Am. Chem. Soc.*, 2016, **138**, 1848.
14 D. T. Gentekos and B. P. Fors, *ACS Macro Lett.*, 2018, **7**, 677.
15 A. Spinnrock and H. Cölfen, *Angew. Chem., Int. Ed.*, 2018, **57**, 8284.
16 X. Liu, C.-G. Wang and A. Goto, *Angew. Chem., Int. Ed.*, 2019, **58**, 5598.
17 A. Rudin, *J. Chem. Educ.*, 1969, **46**, 595.
18 S. S. Rane and P. Choi, *Chem. Mater.*, 2005, **17**, 926.
19 T. Ward, *J. Chem. Educ.*, 1981, **58**, 867.
20 R. Whitfield, N. P. Truong, D. Messmer, K. Parkatzidis, M. Rolland and A. Anastasaki, *Chem. Sci.*, 2019, **10**, 8724–8734.
21 K. Matyjaszewski, *Macromolecules*, 2012, **45**, 4015.
22 M. Ouchi and M. Sawamoto, *Macromolecules*, 2017, **50**, 2603.
23 R. B. Grubbs and R. H. Grubbs, *Macromolecules*, 2017, **50**, 6979.
24 V. Kottisch, D. T. Gentekos and B. P. Fors, *ACS Macro Lett.*, 2016, **5**, 796.
25 R. Whitfield, K. Parkatzidis, M. Rolland, N. P. Truong and A. Anastasaki, *Angew. Chem., Int. Ed.*, 2019, **58**, 13323.
26 Z. Wang, J. Yan, T. Liu, Q. Wei, S. Li, M. Olszewski, J. Wu, J. Sobieski, M. Fantin, M. R. Bockstaller and K. Matyjaszewski, *ACS Macro Lett.*, 2019, **8**, 859.
27 S. Domanskyi, D. T. Gentekos, V. Privman and B. P. Fors, *Polym. Chem.*, 2019, DOI: 10.1039/c9py00074g.
28 Y. Matsushita, A. Noro, M. Iinuma, J. Suzuki, H. Ohtani and A. Takano, *Macromolecules*, 2003, **36**, 8074.
29 A. Noro, M. Linuma, J. Suzuki, A. Takano and Y. Matsushita, *Macromolecules*, 2004, **37**, 3804.
30 J. Neve, J. J. Haven, S. Harrisson and T. Junkers, *Angew. Chem., Int. Ed.*, 2019, **58**, 13869.
31 J.-F. Lutz, M. Ouchi, D. R. Liu and M. Sawamoto, *Science*, 2013, **341**, 1238149.
32 J.-F. Lutz, J.-M. Lehn, E. Meijer and K. Matyjaszewski, *Nat. Rev. Mater.*, 2016, **1**, 16024.

33 B. Oschmann, J. Lawrence, M. W. Schulze, J. M. Ren, A. Anastasaki, Y. Luo, M. D. Nothling, C. W. Pester, K. T. Delaney, L. A. Connal, A. J. McGrath, P. G. Clark, C. M. Bates and C. J. Hawker, *ACS Macro Lett.*, 2017, **6**, 668.
34 B. van Genabeek, B. F. de Waal, B. Ligt, A. R. Palmans and E. Meijer, *ACS Macro Lett.*, 2017, **6**, 674.
35 B. van Genabeek, B. A. Lamers, B. F. de Waal, M. H. van Son, A. R. Palmans and E. Meijer, *J. Am. Chem. Soc.*, 2017, **139**, 14869.
36 B. A. Lamers, B. van Genabeek, J. Hennissen, B. F. de Waal, A. R. Palmans and E. Meijer, *Macromolecules*, 2019, **52**, 1200.
37 A. Das, K. Petkau-Milroy, G. Klerks, B. van Genabeek, R. P. Lafleur, A. R. Palmans and E. Meijer, *ACS Macro Lett.*, 2018, **7**, 546.
38 Y. Jiang, M. R. Golder, H. V. Nguyen, Y. Wang, M. Zhong, J. C. Barnes, D. J. Ehrlich and J. A. Johnson, *J. Am. Chem. Soc.*, 2016, **138**, 9369.
39 M. R. Golder, Y. Jiang, P. E. Teichen, H. V. Nguyen, W. Wang, N. Milos, S. A. Freedman, A. P. Willard and J. A. Johnson, *J. Am. Chem. Soc.*, 2018, **140**, 1596.
40 K. Takizawa, H. Nulwala, J. Hu, K. Yoshinaga and C. J. Hawker, *J. Polym. Sci., Part A: Polym. Chem.*, 2008, **46**, 5977.
41 B. van Genabeek, B. F. de Waal, M. M. Gosens, L. M. Pitet, A. R. Palmans and E. Meijer, *J. Am. Chem. Soc.*, 2016, **138**, 4210.
42 T. Kawai, N. Rahman, G. Matsuba, K. Nishida, T. Kanaya, M. Nakano, H. Okamoto, J. Kawada, A. Usuki, N. Honma, K. Nakajima and M. Matsuda, *Macromolecules*, 2007, **40**, 9463.
43 J. Zhang, K. Tashiro, A. J. Domb and H. Tsuji, *Macromol. Symp.*, 2006, **242**, 274.
44 P. Pan, W. Kai, B. Zhu, T. Dong and Y. Inoue, *Macromolecules*, 2007, **40**, 6898.
45 B. Kalb and A. Pennings, *Polymer*, 1980, **21**, 607.
46 X. Tang, W. Chen and L. Li, *Macromolecules*, 2019, **52**, 3575.
47 R. Zwiers, S. Gogolewski and A. Pennings, *Polymer*, 1983, **24**, 167.
48 S. Z. D. Cheng and B. Wunderlich, *J. Polym. Sci., Part B: Polym. Phys.*, 1986, **24**, 577.
49 J. Yang, Y. Liang, J. Luo, C. Zhao and C. C. Han, *Macromolecules*, 2012, **45**, 4254.